Accepted Manuscript

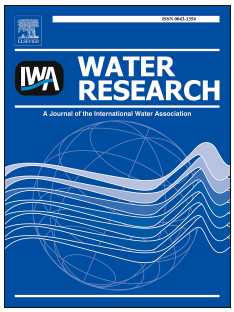

Slippery for scaling resistance in membrane distillation: a novel porous micropillared superhydrophobic surface

Zechun Xiao, Rui Zheng, Yongjie Liu, Hailong He, Xiaofei Yuan, Yunhui Ji, Dongdong Li, Huabing Yin, Yuebiao Zhang, Xue-Mei Li, Tao He

PII: S0043-1354(19)30090-9

DOI: https://doi.org/10.1016/j.watres.2019.01.036

Reference: WR 14402

To appear in: *Water Research*

Received Date: 15 September 2018

Revised Date: 8 January 2019

Accepted Date: 9 January 2019

Please cite this article as: Xiao, Z., Zheng, R., Liu, Y., He, H., Yuan, X., Ji, Y., Li, D., Yin, H., Zhang, Y., Li, X.-M., He, T., Slippery for scaling resistance in membrane distillation: a novel porous micropillared superhydrophobic surface, *Water Research*, https://doi.org/10.1016/j.watres.2019.01.036.

1

2

3

4 Graphic Abstract

5

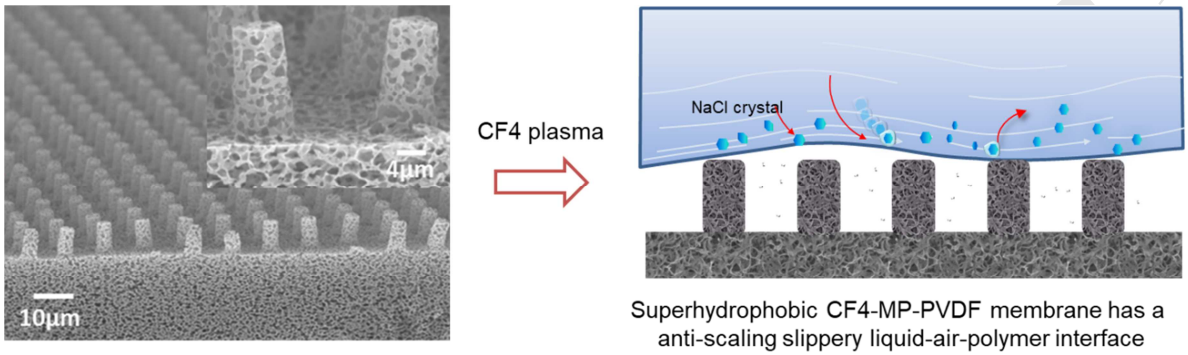

Superhydrophobic CF4-MP-PVDF membrane has a anti-scaling slippery liquid-air-polymer interface

6

7

Slippery for scaling resistance in membrane distillation: a novel porous micropillared superhydrophobic surface

Zechun Xiao[1, 2], Rui Zheng[1, 2], Yongjie Liu[1, 3], Hailong He[3], Xiaofei Yuan[4], Yunhui Ji[5], Dongdong Li[1], Huabing Yin[4*], Yuebiao Zhang[3], Xue-Mei Li[1], Tao He[1,4 *]

[1]Shanghai Advanced Research Institute, Chinese Academy of Sciences, Shanghai 201210, China

[2]University of Chinese Academy of Sciences, Beijing 100049, China

[3]School of Physical Science and Technology, ShanghaiTech University, Shanghai 201210, China

[4]School of Engineering, University of Glasgow, Glasgow, G12 8LT, UK

[5]National Laboratory of Solid State Microstructures, Collaborative Innovation Center of Advanced Microstructures, College of Engineering and Applied Sciences, Department of Materials Science & Engineering, Nanjing University, Jiangsu, 210093, P. R. China

*Corresponding authors: het@sari.ac.cn, Tel: 0086-21-20325162, Fax: 0086-21-20320984

Abstract

Scaling in membrane distillation (MD) is a key issue in desalination of concentrated saline water, where the interface property between the membrane and the feed become critical. In this paper, a slippery mechanism was explored as an innovative concept to understand the scaling behavior in membrane distillation for a soluble salt, NaCl. The investigation was based on a novel design of a superhydrophobic polyvinylidene fluoride (PVDF) membrane with micro-pillar arrays (MP-PVDF) using a micromolding phase separation (μPS) method. The membrane showed a contact angle of 166.0 ± 2.3° and the sliding angle of 15.8 ± 3.3°. After CF_4 plasma treatment, the resultant membrane (CF_4-MP-PVDF) showed a reduced sliding angle of 3.0^o. In direct contact membrane distillation (DCMD), the CF_4-MP-PVDF membrane illustrated excellent anti-scaling in concentrating saturated NaCl feed. Characterization of the used membranes showed that aggregation of NaCl crystals occurred on the control PVDF and MP-PVDF membranes, but not on the CF_4-MP-PVDF membrane. To understand this phenomenon, a "slippery" theory was introduced and correlated the sliding angle to the slippery surface of CF_4-MP-PVDF and its anti-scaling property. This work proposed a well-defined physical and theoretical platform for investigating scaling problems in membrane distillation and beyond.

Keywords: micromolding phase separation; surface pattern; slippery; membrane distillation; scaling; membrane

1. Introduction

Highly saline wastewater streams from steel, chemical, petrochemical, and mining industries are of key concern for environmental and economical sustainability in developing countries (Latorre 2005, Shannon, Bohn et al. 2008, Bouchrit, Boubakri et al. 2015, Choi, Naidu et al. 2018, Deshmukh, Boo et al. 2018). Therefore, concentrating high salinity liquids has become an important task in water treatment. One of the main objectives in recent years is to concentrate close-to-saturation brine until zero-liquid-discharge (Yun, Ma et al. 2006, Shin and Sohn 2016, Junghyun, Heejung et al. 2017). Contemporary technologies, e.g. high pressure reverse osmosis (RO), electrodialysis (ED), mechanical vapor re-compression (MVR) and multi-effect distillation (Li, Wang et al. 2016) have been used, but all have different limitations. For example, RO and ED are powered by electricity, and are normally expensive. MVR and ED not only require high energy but also suffer from corrosion. Membrane distillation (MD) has attracted wide attention for desalinating highly concentrated brine with concentrations up to crystallization (Ji, Curcio et al. 2010, Nghiem, Hildinger et al. 2011, Edwie and Chung 2013, Chen, Lu et al. 2014, Hickenbottom and Cath 2014, Naidu, Jeong et al. 2014, Bouchrit, Boubakri et al. 2015, Chen, Wang et al. 2015, Tian, Yin et al. 2015, Eykens, Hitsov et al. 2016, Gryta 2016, Shin and Sohn 2016, Bouchrit, Boubakri et al. 2017, Chen, Tian et al. 2017, Chen, Zheng et al. 2017, Duong, Hai et al. 2017, Junghyun, Heejung et al. 2017, Choi, Naidu et al. 2018, Julian, Ye et al. 2018, Kim, Kim et al. 2018, Naidu, Zhong et al. 2018).

MD uses low grade heat or sustainable energy (such as solar power) and is potentially an affordable desalination technology (Alkhudhiri, Darwish et al. 2012, Tijing, Woo et al. 2015, Eykens, De Sitter et al. 2017). Normally, a MD system is compact, lightweight, and resistant to corrosion. However, similar to other membranes, MD membranes are prone to fouling, scaling and membrane

wetting (Tijing, Woo et al. 2015), which will lead to deteriorated performance. For high salt solutions, in particular when the concentration of salt approaches saturation, scaling becomes the most serious problem (Ji, Curcio et al. 2010, Gryta 2011, Edwie and Chung 2013, Chen, Lu et al. 2014, Hickenbottom and Cath 2014, Nariyoshi, Pantoja et al. 2016, Bouchrit, Boubakri et al. 2017, Jiang, Tuo et al. 2017, Tang, Iddya et al. 2017, Julian, Ye et al. 2018, Zou, Dong et al. 2018). Crystals attached to the membrane surface alter surface wettability (e.g. from hydrophobic to hydrophilic), allowing continuous crystal growth into membrane pores and consequently membrane wetting (Yun, Ma et al. 2006, Gryta 2008, Ramezanianpour and Sivakumar 2014). Wetted membranes result in free diffusion of salt molecules from the high salinity feed to the permeate, thus reducing membrane rejection. Although the consequence of scaling can be measured, the mechanism governing scaling is unknown. How to prevent scaling remains a significant challenge in membrane technology.

Observations of NaCl scaling have been reported in the literature. When treating 18 wt.% NaCl brine in direct contact membrane distillation (DCMD), a critical size of 25 μm was found for the crystals on the PVDF membrane surface, which acted as initial growth sites and led to the full membrane coverage (Chen, Lu et al. 2014). Single NaCl crystals of 40 μm were also reported in a membrane distillation-crystallization (MDC) process, where about 9 to16% of the total crystals were on the membrane surface and the piping (Nariyoshi, Pantoja et al. 2016). Scaling often occurred when the feed reached saturation (Bouchrit, Boubakri et al. 2015, Gryta 2016, Bouchrit, Boubakri et al. 2017). Injection of air (Choi, Choi et al. 2017) and increase of the feed flow velocity (Naidu, Jeong et al. 2014, Choi, Choi et al. 2017) can mitigate scaling. However, when optimization of process parameters such as flow rate and temperature reversal were used to mitigate rapid flux decline in concentrating salt lake brine, there was little successes (Hickenbottom and Cath 2014).

Instead of optimizing process parameters, membrane modification provides another important route to mitigate or prevent scaling. An electrically conducting membrane surface can be made by coating a carbon nanotube/poly(vinyl alcohol) (PVC) layer onto a polypropylene support, which can effectively dissolve silicate scale during desalination of geothermal brine (Tang, Iddya et al. 2017). It has been shown that air bubbles can be created on the superhydrophobic surface of a perfluorodecyl acrylate modified poly(vinyldene fluoride) PVDF membrane (i.e. via initiated chemical vapor deposition, iCVD), which can suppress MD fouling despite increased crystal formation (Warsinger, Servi et al. 2016). However, in another study, a superhydrophobic membrane prepared by coating TiO_2 nanoparticles on a PVDF electrospun nanofiber support followed by chemical fluorosilanization, promoted more uniform and slower crystal formation and removal of the crystal deposition was easy (Razmjou, Arifin et al. 2012, Meng, Ye et al. 2014, Meng, Ye et al. 2015).

The majority of research on superhydrophobic membranes are based on chemical modification and /or the design of hierarchical structure (Razmjou, Arifin et al. 2012, Wei, Zhao et al. 2012, Meng, Mansouri et al. 2014, Meng, Ye et al. 2014, Yang, Li et al. 2014, Meng, Ye et al. 2015, Tian, Yin et al. 2015, Yang, Tian et al. 2015, Lee, An et al. 2016, Tijing, Woo et al. 2016, Warsinger, Servi et al. 2016, Ren, Xia et al. 2017). Contradictory results were often observed (e.g. the examples above). These might be due to variations in the feed as well as undefined surface morphology. An intuitive assumption in MD is the existence of a static membrane/liquid interface. Therefore, it has been believed that mimicking the hierarchical structure of lotus leaves could provide an anti-fouling solution. However, actual fouling/scaling in MD occurs at triple-phase interfaces consisting of liquid phase (feed) – air phase (in pores) – solid phase (polymer). If the tri-phase interfaces are not always static, scaling can occur in different ways. The mechanisms underlying fouling and scaling in MD is

105 highly complex. To address this challenge, our vision is to design a simple, but structurally
106 well-controlled membrane surface that can modulate the interface properties and provide a dynamic
107 contact line between the membrane and water phase.

108 Advances in nanofabrication technology have been used to create superhydrophobic surfaces (Li,
109 Reinhoudt et al. 2007, Xue Mei Li 2007, Li, He et al. 2008) and surfaces with multidimensional
110 roughness (Kim, Lee et al. 2016). A recent study shows that MD membranes patterned with a groove
111 structure have a weak hydrophobic interaction with BSA proteins and hence low fouling propensity
112 (Xie, Luo et al. 2017). However, since the evaluation was in static conditions, information on scaling
113 was not available. Similarly, corrugated PVDF membranes demonstrate the ability to alleviate salt
114 deposition and fouling in DCMD of real seawater (Kharraz, Bilad et al. 2015), but the dynamics of
115 scaling was unknown.

116 Here, we attempt to understand the dynamic mechanisms of scaling at the liquid-air-solid
117 interface in MD. For the first time, a patterned superhydrophobic PVDF membrane with porous
118 micropillars was prepared via a micro-molding phase separation (μPS) technique. A similar
119 technique has been used to create macro-patterned surfaces for pressure driven membranes (Çulfaz,
120 Rolevink et al. 2010, Çulfaz, Haddad et al. 2011, Çulfaz, Wessling et al. 2011, Hashino, Katagiri et al.
121 2011, Won, Lee et al. 2012, Jamshidi Gohari, Lau et al. 2013, Lee, Won et al. 2013, Gençal, Durmaz
122 et al. 2015, Maruf, Greenberg et al. 2016, Won, Jung et al. 2016, ElSherbiny, Khalil et al. 2017).
123 However, pressure driven processes only involve a liquid-solid interface with a convective flow of
124 liquid across the membrane. Therefore, it is fundamentally different from the vapor diffusion-based
125 MD process. Here, porous micro-pillar formation together with CF_4 plasma treatment allowed the
126 creation of a superhydrophobic PVDF membrane, which is employed to investigate: (1) the

relationship between the micro-pattern and the hydrophobicity of the membrane surface; and (2) the relationship between the micro-pattern and the scaling property in DCMD for highly concentrated NaCl solutions. The superhydrophobic membrane demonstrated excellent anti-scaling properties when used to treat a saturated NaCl solution by DCMD. The results lend us to propose a "slippery surface" as a dynamic means of preventing scaling in MD. The novel multiscale hierarchical surface illustrated in this work also offers a promising platform for understanding and mitigating the scaling and fouling problems in other processes beyond MD.

2. Materials and methods

2.1 Materials and chemicals

PVDF (Solef 1015) was kindly supplied by Solvay. N, N-Dimethylacetamide (DMAc, AR) and Diethylene glycol (DEG, AR) were purchased from Sinopharm Chemical Reagent Co. Ltd and used without further purification. The silicon wafer mold with a pillar array was designed in house. The dimensions of the pillars are 5 μm in diameter (D), 10 μm in height (H) and 10 μm in period (P) (Fig.1). A commercial flat sheet polyvinylidene fluoride membrane (abbreviated as C-PVDF, GVHP, Millipore, USA) with a nominal pore size of 0.22 μm and thickness of 125 μm was used as a benchmark.

2.2 Fabrication of polydimethylsiloxane (PDMS) mold

Oligomer PDMS and the curing agent (SYLGARD 184, Dow Corning Co. Ltd) were pre-mixed at a weight ratio of 10:1. After de-gassing in vacuum for 10 min, the mixture was cast onto the silicon wafer template. Then the wafer and the PDMS solution was transferred into a vacuum oven and cured for 3 hours at 60°C. The PDMS replica was then peeled off and stored in a clean container.

The entire process was carried out in a clean room.

2.3 Fabrication of MP-PVDF membrane

A PVDF casting solution (PVDF/DEG/ DMAc, 15/27.4/57.6 wt.%) was prepared by mixing the components in a flask at 90 ^{o}C and agitated for 12 h. The polymer solution was then filtered using a metal filter of 40 µm. The casting solution was kept at 90 ^{o}C to de-gas. Fig. 1 shows the procedure for the fabrication of micro-pillar PVDF membranes and details are as follows.

An appropriate amount of the PVDF solution was spread uniformly on the PDMS replica on top of a glass plate to a thickness of 600 µm using a home-made stainless-steel casting knife. The solution was exposed to water vapor for 10 s (10 cm above a coagulation water bath, 75^{o}C) and then immersed in the coagulation bath for 15 minutes to induce precipitation. Upon precipitation, the membrane delaminated from the replica spontaneously. After rinsing with water to remove solvent and additives, ethanol was used to rinse the membrane before being dried in a vacuum oven at ambient temperature for 48 h. The resultant membrane is denoted as micro-pillared PVDF membrane (MP-PVDF).

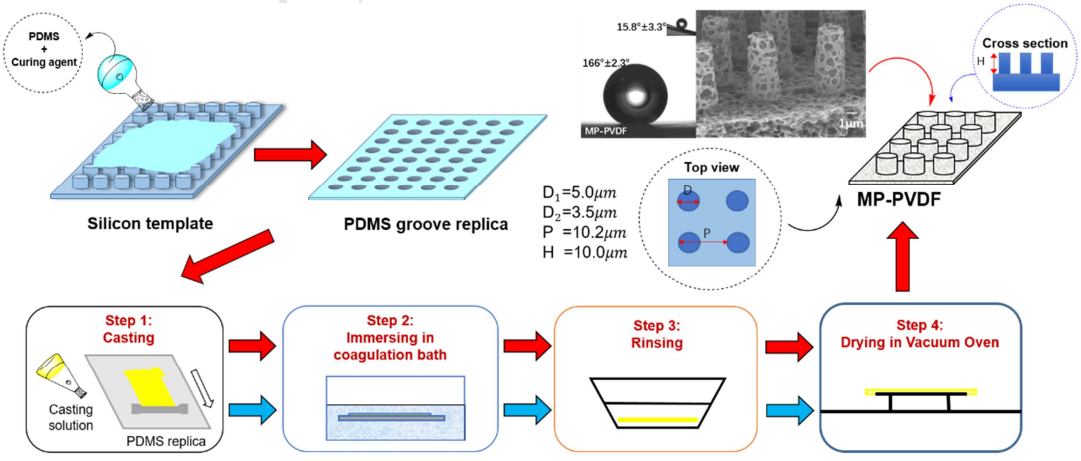

Fig. 1 Schematic for the fabrication of micro-pillar PVDF membranes (MP-PVDF). The silicon

167 wafer mold has pillars with the dimension of 5 µm (diameter), 10 µm (height) and 10 µm (period).

168 2.4 Membrane modification by CF4 plasma treatment

169 MP-PVDF membrane was further treated with CF_4 plasma (an IoN40 plasma system, PVA
170 Tepla Co.Ltd) to improve its hydrophobicity based on our previous methods (Wei, Zhao et al. 2012,
171 Yang, Li et al. 2014, Yang, Tian et al. 2015, Chen, Tian et al. 2017, Chen, Zheng et al. 2017). In
172 brief, the substrate was cleaned first under argon plasma at 45W for 15s and then in CF_4 gas at a flow
173 rate of 120 cm^3/min (SCCM) at 200W for 15 min. After the CF_4 modification, the chamber was
174 cleaned using an O_2 plasma at 200W for 15 min to avoid any CF_4 deposition on the electrodes.

175 2.5 Membrane characterization

176 Water contact angle (CA) and sliding angle (SA) of the samples were measured using a contact
177 angle goniometer (Maist Drop Meter A-100P) via the sessile drop method. The tilt angle at which the
178 droplet started rolling off the surface was denoted as the sliding angle. Pore size and pore size
179 distribution were analyzed using porometry (Porolux 1000, Supplementary information Method S1)
180 (Wei, Zhao et al. 2012, Yang, Li et al. 2014, Yang, Tian et al. 2015, Chen, Tian et al. 2017, Chen,
181 Zheng et al. 2017). Scanning electron microscopy (HITACH TM-1000 and FEI Nova Nano SEM
182 450) was used to characterize membrane morphology. The sample was sputtered with a thin layer of
183 gold in a vacuum prior to SEM characterization.

184 2.6 MD performance

185 A bench scale DCMD unit (Supplementary Data Fig. S1) developed previously (Wei, Zhao et al.
186 2012, Yang, Li et al. 2014, Yang, Tian et al. 2015, Chen, Tian et al. 2017, Chen, Zheng et al. 2017)
187 was used to evaluate scaling on the membranes using 4 wt.% or 25 wt.% NaCl solutions. For the
188 MP-PVDF and CF_4-MP-PVDF membranes, the side with pillars was in contact with the feed. The

conductivity of the permeate was regularly measured to identify the point when salts from the feed penetrate to the permeate. Since 25 wt.% is close to the saturated concentration for a NaCl solution, the experimental duration was significantly reduced. The feed and the permeate temperatures were maintained at 60 ± 0.3 °C and 20 ± 0.3 °C respectively. The flux (J, kg/m^2·h) was calculated based on equation (1):

$$J = \Delta m / A \Delta t. \qquad \text{Equation (1)}$$

Where Δm (kg) is the amount of water transported from the feed to the permeate, Δt the interval of the collection (h) and A the membrane area (m^2).

3. Results and discussion

3.1 Morphology of the MP-PVDF membrane

Fig. 2 shows the SEM images of the top, bottom and cross-section of the commercial PVDF (C-PVDF) and micro-pillar PVDF (MP-PVDF) membrane. Both membranes show a porous top and bottom surface, as well as a macroporous cross-section. The surface porosity and pore size of MP-PVDF membranes appears to be lower than C-PVDF membranes. In addition, MP-PVDF membranes contain porous pillar arrays with open structure throughout (Fig. 2, inserts). For the sake of clarity, the membrane surface facing the feed is denoted as the top surface. In this study, the top surface of the MP-PVDF membrane (Fig. 2) was the one in contact with the PDMS replica. During membrane formation, phase separation started from the open surface of the polymer solution; instantaneous demixing occurred at the water/polymer solution interface, resulting in a finger-like macrovoid structure (i.e. MP-PVDF cross-section in Fig. 2). However, solvent and additives from the polymer solution within the PDMS replica had to diffuse through the whole membrane to the water

bath and therefore it was a slow process. This allowed the polymer-lean phases to grow and eventually enlarge into micropores (He, Mulder et al. 2003, Li, Ji et al. 2008, Ji, Li et al. 2010, Li, Ji et al. 2010). The interconnected porous structure in the top surface of the PVDF membrane is due to the competition between the solid-liquid phase separation and liquid-liquid separation for a semi-crystalline polymer (Xing, Song et al. 2016). The open porous surface in the pillars is of particular interest for creating a superhydrophobic surface.

The MP-PVDF membrane features an array of conical pillars of 5 μm at the bottom (i.e. the part connected to the bulk membrane) and 3.5 μm at the tip. Compared to the original pillar structure on the silicon mold, this reduction at the tip is likely caused by membrane shrinkage during phase separation. Nevertheless, the height and period for pillars on the membrane are the same as the designed silicon mold, i.e. 10 μm in both height and period.

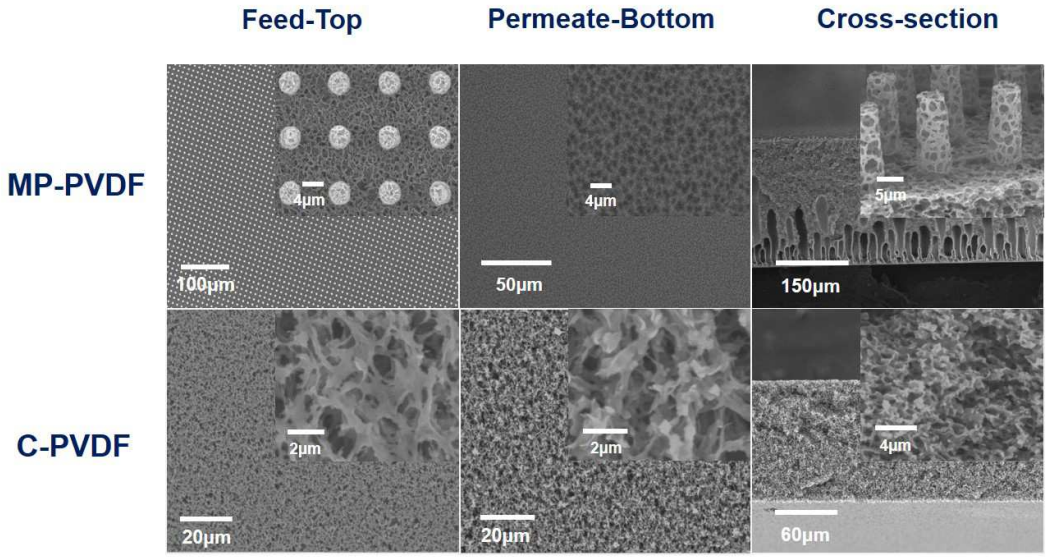

Fig. 2 SEM images of MP-PVDF and C-PVDF membranes. Feed-Top, Permeate-bottom and cross section. The top surface of MP-PVDF was slight tilted for a better view. Inserts are enlarged views.

As listed in Table 1, the MP-PVDF membrane has a thickness of ~264 μm, whereas the commercial PVDF membrane (C-PVDF) is of 130 μm. Attempts to reduce this thickness could be possible by controlling the casting process. Slightly higher porosity is found in MP-PVDF membranes (~79 %) than C-PVDF membrane (75 %), indicating a more open porous substrate in MP-PVDF. However, the mean pore size of MP-PVDF membranes (0.120 μm) is smaller than C-PVDF membranes (0.230 μm). Interestingly, the contact angle for MP-PVDF membranes (166.0±2.3°) is significantly higher than that of C-PVDF membranes (139.2±3.7°). The CF_4 plasma treatment may fluorinate membrane surfaces by F atom insertion or deposition of Teflon polymers (Yang, Li et al. 2014, Tian, Yin et al. 2015, Yang, Tian et al. 2015). This leads to a slightly enlarged mean pore size (i.e. from 0.120 μm to 0.201 μm), and further increased contact angle (i.e. from 166° to 176°). As shown in Fig. S2 (Supplementary Data) , C-PVDF membrane possessed a narrow distribution of pore size, whereas C-PVDF and CF_4-MP-PVDF showed a relatively large pore size distribution.

The most striking difference is the sliding angle: C-PVDF membranes showed no sliding angle below 90°; MP-PVDF membranes showed a sliding angle of 15.8°; and CF_4-MP-PVDF showed a sliding angle of only 3.0°. The surface of CF_4-MP-PVDF membrane was so water repellent that a water droplet stuck to the needle rather than the membrane surface during the contact angle test. When the water droplet was released from the needle by a gentle flick, it rolled off the surface upon slight tilting. The surface energy follows a reverse order compared to the contact angle: C-PVDF membrane show the highest surface energy of 72 mJ/m^2, and CF_4-MP-PVDF membranes show the lowest energy of 0.27 mJ/cm^2. This water repelling property and low surface energy of the CF_4-MP-PVDF membrane surface are not trivial characteristics, which are most probably related to

249 the scaling/fouling process as shown in the experiments below.

250

251 Table 1. Characteristics of the C-PVDF, MP-PVDF and CF_4-MP-PVDF membranes.

Membrane	C-PVDF	MP-PVDF	CF_4-MP-PVDF
Thickness/ μm	132 ± 3	263 ± 2	264 ± 2
Mean pore size/ μm	0.230 ± 0.0020.235±0.013	0.078 ± 0.0120.120±0.005	0.073 ± 0.0090.201±0.013
Porosity (%)	75.3±2.1	79.6±3.7	78.9±5.3
Contact angle/^{o}	139.2±3.7	166.0±2.3	175.6±1.3
Sliding angle /^{o}	>90	15.8±3.3	3.0±0.8
Surface energy (mJ/m^2)*	71.8±2.4	47.3±0.6	0.27±0.12

252 * Supplementary information Method S2 for determination of surface energy.

253

254 Both MP-PVDF and CF_4-MP-PVDF membranes can be categorized as superhydrophobic due to
255 their high contact angle and low sliding angles. The commercial PVDF membrane has a very open
256 porous surface, but its contact angle was only 139°, and its sliding angle is above 90°. Water droplets
257 on a hydrophobic surface are normally considered as either in the Cassie-Baxter state or in the
258 Wenzel state (Li, Reinhoudt et al. 2007, Xue Mei Li 2007, Li, He et al. 2008, Tian, Li et al. 2015).
259 The difference between the two states is the contact areas between the water and the solid substrate:
260 The Wenzel state is characterized by a larger contact area and more interaction between the liquid
261 phase and solid phase, whereas air pockets between the liquid and solid phase are expected for the

Cassie-Baxter state. Sliding angle is an indirect macroscopic feature indicating interaction between a surface and a water droplet. A sliding angle above 90°, is an indication of strong interaction between the surface and water. This minor, but very important information shows that the surface characteristics of the C-PVDF membrane is different from that of micropillared membrane (MP-VPDF and CF_4-MP-PVDF). For C-PVDF membranes, the water contact angle was found to be much higher than 90°, and no obvious wetting upon immersion in water was observed. However, if comparing to MP-PVDF and CF_4-MP-PVDF membranes with a high contact angle and low sliding angle, it is likely that water on C-PVDF surface is in a meta-Cassie-Baxter state with partial wetting. The cause might be related to the surface morphology: C-PVDF membrane has a homogeneous porous surface, but both MP-PVDF and CF_4-MP-PVDF have pillars with higher surface porosity. The state of water in contact with the membrane surface is not clear yet at this stage, but worthy of future analysis. Previous work on MD membranes with a superhydrophobic or omniphobic surface only considered static water contact angles, and did not measure sliding angles (Wei, Zhao et al. 2012, Lin, Nejati et al. 2014, Yang, Li et al. 2014, Nejati, Boo et al. 2015, Tian, Yin et al. 2015, Yang, Tian et al. 2015, Boo, Lee et al. 2016, Boo, Lee et al. 2016, Lee, Choi et al. 2016, Lee, An et al. 2016, Lee, Boo et al. 2016, Tijing, Woo et al. 2016, Wang, Hou et al. 2016, Wang, Jin et al. 2016, Chen, Tian et al. 2017, Chen, Zheng et al. 2017). In the MD process, water flows along the membrane surface, and thus behaves dynamically. Increasing the feed flow rate was reported to mitigate scaling (Naidu, Jeong et al. 2014, Choi, Choi et al. 2017), which might be relevant to the dynamic behavior at the interface between water and membrane.

283 3.2 MD performance

284 Fig. 3 shows the flux and permeate conductivity using C-PVDF, MP-PVDF and CF_4-MP-PVDF
285 membranes. An initial feed solution of 25 wt.% NaCl was concentrated until changes in the flux or
286 permeate conductivity occurred. We intentionally selected this close-to-saturation concentration to
287 reduce the experiment time. With increased concentration, the C-PVDF membrane showed a gradual
288 decrease in flux. When the concentration factor (i.e. the ratio of the salt concentration during the
289 process to its initial concentration in the feed) reached about 1.1, the flux suddenly dropped to zero.
290 A similar trend was found for the MP-PVDF membrane, but at a concentration factor of about 1.2. In
291 contrast, CF_4-MP-PVDF membranes maintained a surprisingly stable flux at much higher
292 concentration factors (i.e. 1.76). Initial tests using a 4 wt.% NaCl feed solution showed no obvious
293 variations in both flux and permeate conductivity for the three membranes. They were intact and
294 remained integral (Supplementary information, Fig. S3). Reproducibility of the DCMD results was
295 confirmed as shown in Supplementary Data, Fig. S4.

296 In terms of flux, CF_4-MP-PVDF showed a slightly higher initial flux than MP-PVDF. This is
297 probably due to the enlarged effective evaporation surface area at the liquid-air-solid interface which
298 contributed to the increased water flux (Yang, Li et al. 2014, Yang, Tian et al. 2015). This difference
299 gradually disappeared when the concentration factor reached 1.1, and after that both CF_4-MP-PVDF
300 and MP-PVDF membranes showed a similar flux.

301 In the case of permeate conductivity, very different results were obtained (Fig. 3B). The
302 permeate conductivity of C-PVDF membranes increased gradually until a concentration factor of 1.1
303 (i.e. the flux declined to zero). Similar trend was observed for MP-PVDF membranes. For
304 CF_4-MP-PVDF, the permeate conductivity increased continuously throughout the whole process

until 350 μS/cm, without obvious sacrificing in MD flux. This phenomenon is striking in that saturated NaCl feed would generally cause instantaneously scaling and dramatic flux decline in MD (Tun, Fane et al. 2005, Gryta 2010, He, Gilron et al. 2013). Increase in permeate conductivity is an indication of diffusion of NaCl from saturated feed to the permeate; however, at the concentration factor of 1.76, the CF_4-MP-PVDF membrane showed a rejection of 99.9% (Supplementary Data Fig. S5). Although this value is very high, rigorous analysis would claim that current membrane is not perfect or other unknown mechanism exists. Minor defects in the membrane allow diffusion of NaCl from feed to permeate; at low feed NaCl concentration, the diffusion of NaCl is minor thus the permeate conductivity does not show appreciable increase; but at saturation, diffusion of NaCl was noticed in the permeate. Besides the contribution of defects, the other contribution might be that the NaCl aerosols, generated at the interface from the saturated feed, eventually pass the porous hydrophobic pores and end in the permeate. Sea salt aerosols (SSA) have been routinely found at the marine boundary(Tyree, Hellion et al. 2007, Jentzsch, Ciobotă et al. 2011). We have to admit that this hypothesis is of no direct proof yet and requires further scientific investigation.

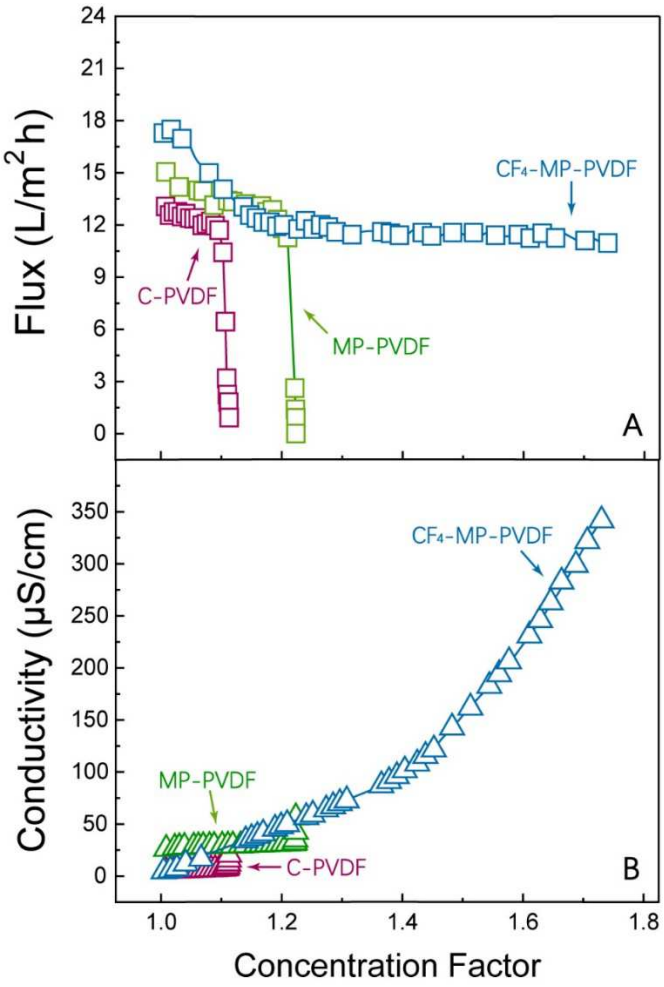

Fig. 3 DCMD performances of C-PVDF, MP-PVDF and CF_4-MP-PVDF membranes with an initial 25wt. % NaCl feed solution. A and B: Water flux and permeate conductivity of three membranes as a function of concentration factor. The feed temperature was maintained at 60 ^{o}C and the permeate temperature at 20 ^{o}C. The concentration factor is defined as the ratio of the salt concentration in the feed during the process to the initial salt concentration (i.e. 25 wt.% NaCl).

After the DCMD experiment, membrane samples were removed from the test cell and characterized as shown in Fig. 4. The contact angle for both C-PVDF and MP-PVDF membranes, was significantly reduced. The sliding angle of MP-PVDF membranes increased dramatically from 15.8° to above 90°, indicating that the surfaces became sticky to water. In contrast, the contact angle

of CF_4-MP-PVDF membranes remained unchanged, but the sliding angle slightly increased from 3.3° to 10.5°. Optical images showed that the surfaces of CF_4-MP-PVDF on both feed and permeate sides remained clean. However, the surfaces of both C-PVDF and MP-PVDF membranes showed NaCl crystals (as highlighted by the red circles in Supplementary Data Fig. S6). This observation was further confirmed by the SEM images (Fig. 4B): a layer of NaCl crystals of various sizes were observed on the C-PVDF surface and some cubic crystals even imbedded in the middle of the support; furthermore, even permeate surface showed some cubic particulates which would be NaCl crystals. The surface of MP-PVDF was fully covered by a thick layer of NaCl crystals, and no full-sized pillars could be identified, no obvious large NaCl crystals were found in the porous structure.

Obviously, the scaling behavior of three membranes in concentrating the NaCl solution was different, caused by the different membrane morphology and/or chemistry. A large thick layer of crystals on MP-PVDF membrane indicates that the NaCl was mainly at the membrane surface (and in the original open space between pillars), but for C-PVDF membranes, liquid might have penetrated into the support; or C-PVDF membrane was partially wetted. In MD process, external concentration polarization and temperature polarization tend to increase the possibility of NaCl nucleation at the membrane surface(Schofield, Fane et al. 1987, Martínez-Díez and Vázquez-González 1999, Yang, Tian et al. 2015). Consequently, at a concentration factor of 1.1, the feed bulk reached salt concentration above the saturation point (Godoy, Carvalho et al. 2017); at the same time, the salt concentration at the membrane/liquid interface is even higher than the bulk. It is thus probable that the nucleation of NaCl occurs at membrane surface before in the bulk. Therefore, the scaling for both C-PVDF and MP-PVDF membranes is initiated from the surface rather than in

353 from the bulk feed. Difference in the extend of scaling for C-PVDF and MP-PVDF membranes could
354 be resulted from the different surface morphology. The micropillars in the MP-PVDF membranes
355 surface tend to create micro turbulence (Lee, Won et al. 2013, Jung, Won et al. 2015, Won, Jung et al.
356 2016); the thick crystal layer is most probably originated from this turbulence which lead to quick
357 nucleation of NaCl crystals, thus coverage of the membrane surface. However, C-PVDF membrane
358 has rather homogeneous surface pores; nucleation of NaCl crystals lead to wetting, resulted in
359 crystals in the support layer. This phenomenon has been reported and nucleation and wetting of the
360 polypropylene membranes by NaCl concentrated solution. As a consequence, the MD flux declined
361 as soon as the membrane was wetted (Gryta 2002, Gryta 2002).

362 Very interesting observation was that CF_4-MP-PVDF membrane did not show any scaling or
363 fouling, and the MD flux was very stable at a concentration factor of 1.78, far above the saturation.
364 Assuming that the feel did not form NaCl crystals in the bulk, the solution was then super-saturated.
365 Although supersaturation without crystallization is possible (He, Sirkar et al. 2009, He, Sirkar et al.
366 2009), one would expect that the vapor pressure of the supersaturated solution decreases;
367 consequently, the MD flux would gradually decline. Therefore, the stable MD flux was an indication
368 of constant feed NaCl concentration. This means that there probably was crystallization of NaCl
369 from the feed solution after the solution was supersaturated. However, no suspension was observed
370 in the bulk feed caused by the crystallization of NaCl in the experiment. The phenomenon will be
371 further addressed in the next session. To unravel this puzzle is scientifically interesting and
372 challenging, at present, we are not able to identify the origin of scalant yet. An online monitoring
373 method will be required and the effect of the membrane surface morphology and chemistry on the
374 scaling formation will be clarified and published in the future.

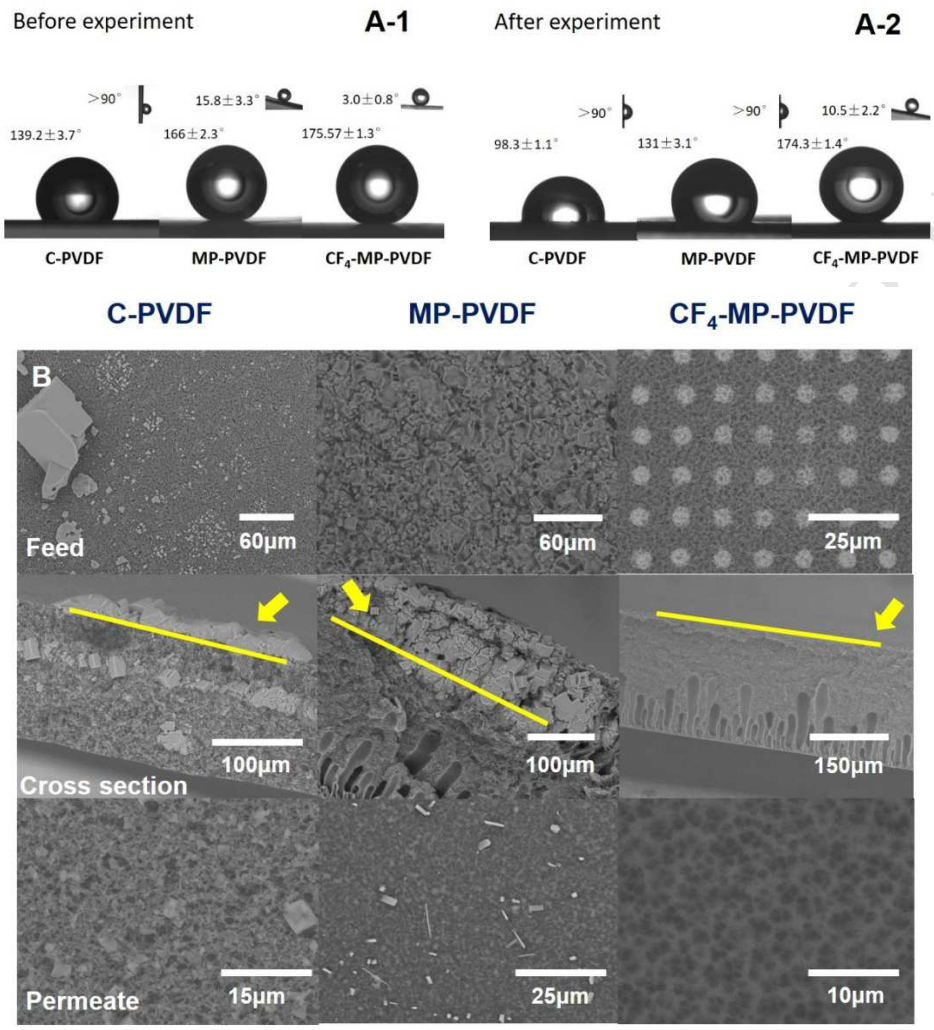

Fig. 4 Characteristics of C-PVDF, MP-PVDF and CF_4-MP-PVDF membranes before and after DCMD test. (A-1) and (A-2): contact angles and sliding angles of three membranes before and after DCMD; (B): SEM images of the surfaces and cross-section. For the cross-section images, arrows and lines indicate the membrane surface at the feed side. C-PVDF and MP-PVDF membranes showed aggregates of crystals.

3.3 Origin of anti-scaling: hypothesis

The reduction in the contact angle is obviously caused by the scaling by NaCl. Upon saturation, C-PVDF was scaled by NaCl crystals, followed by a rapid flux decline to zero. Although the

MP-PVDF membrane showed a delay to a concentration factor of 1.2, scaling was inevitable (Fig. 3 and Fig. 4 B). With such a harsh saturated solution, the clean surface of CF_4-MP-PVDF on the feed side demonstrated a surprising anti-scaling property. CF_4-MP-PVDF membranes have a very low sliding angle (Fig. 4 A-1), and their surface was repellent to water droplets. Correlation between the two phenomena raised questions: Did the water "feel" slippery at the liquid-air-polymer interface? Did this prevent the attachment of nucleation of NaCl crystals or attachment of crystals to the interface, leading to the CF_4-MP-PVDF membranes being resistant to scalant even in a supersaturated solution? In our research, however, the results of the contact angle and sliding angle have already given hints on the dynamic behavior in MD. We utilized a peristaltic pump in the experiment to give extra force to increase the release of the matters from the membrane surface for reduction of scaling. Special care was taken to prevent bulky amount of air flow into the system; but sporadically some bubbles could be visualized to enter the module. As shown in Video S1 (Supplementary information), interesting phenomena on membrane surfaces in the feed were observed: (1) for MP-PVDF membrane, bubbles were constantly seen, slowly moving along the surface in the direction of the flow; (2) for C-PVDF membrane, bubbles were seen, but mostly remaining in place; sporadically some small air bubble flowing into the module moved along the flow; (3) for CF_4-MP-PVDF membranes (the video was modified into slow motion for a clear view), there were bubbles which appeared and disappeared constantly following the pulses of the pump; moreover, a large motion of liquid-air interface was observed along the membrane surface. Above difference, though preliminary and qualitative, enlightens us on an important factor for scaling resistance for CF_4-MP-PVDF membrane.

Hereby, we propose a hypothesis that the dynamics at the liquid-air-polymer interface largely

409 dictate scaling. We first define a “stick” or “slippery” surface based on sliding angle. C-PVDF was
410 defined as a “sticky” surface since its sliding angle is above 90° (Fig. 4 A-1). This “sticky” surface
411 might cause non-slip of the liquid phase at the interface. For a superhydrophobic surface with a
412 very low sliding angle, CF_4-MP-PVDF is defined as a “slippery” surface since its sliding angle is
413 far below 10° (Fig. 4 A-1). This means that water actually “floats” above the air-polymer surface.
414 For MP-PVDF membranes, the magnitude of stickiness or slipperiness lies between the two
415 extremes.

416 Slippery surface (SLIPs) with liquid infusion has been reported for inhibition of ice nucleation
417 or anti-ice/anti-frost performance(Kim, Wong et al. 2012, Kim, Kreder et al. 2013, Wilson, Lu et al.
418 2013). The slippery surface we proposed could be identified as “an air/vapor infused surface”. This
419 logic deduction would lead to similar concept of anti-scaling for NaCl crystals. This engineered
420 slippery liquid/air/solid interface is theoretically resistant to any crystalline particulates. We admit
421 that the effect of the chemistry nature and nucleation/growth of the crystals to scaling for
422 micropillared membrane is unknown and worth of further investigation. Because MD involves
423 mass transfer, concentration and temperature polarization, it is much more complicated than the
424 SLIPs surface created by liquid infusion(Kim, Wong et al. 2012, Kim, Kreder et al. 2013, Wilson,
425 Lu et al. 2013). At present, we are conducting non-intrusive observation the formation of scaling
426 and evidence will be reported in the near future (Fortunato, Jang et al. 2018, Lee, Jang et al. 2018).

427 Consequently, a slippery surface is hypothesized to be scaling resistant because dynamically the
428 liquid remains floating above the polymer phase; or the fluid solid interface is constantly changing;
429 in other words, the liquid feels slippery at the interface. The observation of a large air/liquid
430 interface flowing along the membrane surface was an indirect proof. However, the direct

consequence is that, no crystals directly contact the polymer phase even though there are NaCl crystals in the liquid phase. Thus, the chance for scaling is low (Fig. 5). For CF_4-MP-PVDF membrane, due to the constantly moving interface, very limited interaction of the liquid and the membrane polymer could not allow the formation of nuclei on the membrane surface; even if the solution contains crystals, it is also very difficult to attach to the surface. On the contrary, for a "sticky" surface, there exists a rather static liquid-air-polymer interface; above saturation, the chance for nucleation and growth on the membrane surface increases; Driven by the concentration and temperature polarization, NaCl crystals would form on the surface and so does scaling. The in-situ observation of the dynamic scaling process at the interface remains challenging. We are currently working with other scientists using optical coherence tomography (OCT) (Fortunato, Jang et al. 2018, Lee, Jang et al. 2018) to further confirm the observation and compare different surface morphology on the scaling for various inorganic salts.

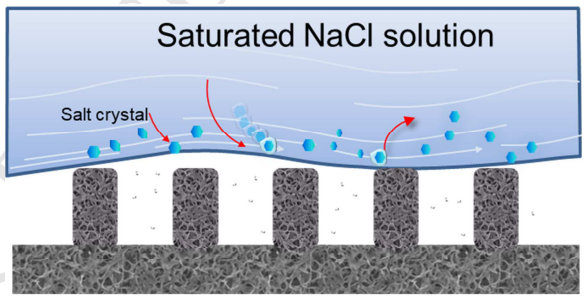

Fig. 5 Schematic of the slippery interface in relation to anti-scaling for CF_4-MP-PVDF membrane.

The other quantitative measure of the slipperiness of hydrophobic soft polymeric membrane surfaces has not yet been established in the literature. Nevertheless, the measurement of

449 slipperiness of superhydrophobic surface has been reported as the slip length based on Navier's
450 model (Granick, Zhu et al. 2003, Choi, Ulmanella et al. 2006). Measurement of the slip length of a
451 surface would indirectly support the present correlation of slip and scaling. Beyond scaling, the
452 investigation of current slippery surface is useful for quantifying the flow resistance of the inner
453 surface of a channel (Choi, Ulmanella et al. 2006, Truesdell, Mammoli et al. 2006, Daniello,
454 Waterhouse et al. 2009, Haase, Wood et al. 2016). Low friction has been shown at a nanopatterned
455 surface (Cottin-Bizonne, Barrat et al. 2003), which might be related to the formation of
456 "nanobubbles" that gave rise to reduced friction resulting in a slippery surface (Tyrrell and Attard
457 2001, Shin, Park et al. 2015). As shown in video S1 (Supplementary information), we didn't
458 observe nanobubbles, but a moving air/liquid interface along the superhydrophobic CF_4-MP-PVDF
459 membrane surface. This observation provided a qualitative proof of the possible slippery character
460 at the interface. Yet, the scientific evidence requires further experimental verification of the slip
461 length and simulation of the flow pattern. The fundamental dynamic mechanism of scaling in
462 membrane distillation could then be clarified. Understanding the dynamic scaling resistance might
463 also shed light on fouling by other organic matter. This assumption lies in the probability of
464 interaction between the foulant (in the feed) and the membrane materials. If direct contact between
465 the membrane materials and the feed fouling is largely suppressed, fouling resistance might be
466 observed.
467

468 **4. Conclusion remarks**

469 Superhydrophobic polyvinylidene fluoride (PVDF) membranes with micropillar arrays

(MP-PVDF) were created via a micromolding phase separation (μPS) technology, providing a simple method for creating well-controlled surface morphology. With an additional CF_4 plasma treatment of MP-PVDF, the resultant CF_4-MP-PVDF had a significantly increased contact angle (174^o) and decreased sliding angle (3.0^o). This CF_4-MP-PVDF membrane showed less scaling upon concentrating highly saline NaCl solution (25 wt.%) by direct contact membrane distillation. In contrast, both commercial PVDF and MP-PVDF membranes showed severe scaling followed by flux reduction. Membrane autopsy showed that scaling by NaCl crystals and possible wetting occurred in C-PVDF and MP-PVDF, but not CF_4-MP-PVDF membranes. Visual observation of a floating water/air interface in CF_4-MP-PVDF membranes qualitatively demonstrated that a slippery surface might contribute to resistance to scaling. We hypothetically correlate the sliding angle to the slippery surface of CF_4-MP-PVDF and its anti-scaling properties. This work may provide a platform and methodology for understanding scaling beyond membrane distillation.

5. Acknowledgements

The research is supported by Newton Advanced Fellowship (Grant No. NA170113) and National Natural Science Foundation of China (No. U1507117, 21676290, 51861145313). Zechun Xiao and Rui Zheng contributed equally to the experimental work.

6. References

Alkhudhiri, A., N. Darwish and N. Hilal (2012). "Membrane distillation: A comprehensive review." Desalination **287**: 2-18.

Boo, C., J. Lee and M. Elimelech (2016). "Engineering Surface Energy and Nanostructure of Microporous Films for Expanded Membrane Distillation Applications." Environmental Science & Technology **50**(15): 8112-8119.

492 Boo, C., J. Lee and M. Elimelech (2016). "Omniphobic Polyvinylidene Fluoride (PVDF) Membrane
493 for Desalination of Shale Gas Produced Water by Membrane Distillation." Environ Sci Technol
494 **50**(22): 12275-12282.
495 Bouchrit, R., A. Boubakri, A. Hafiane and S. A.-T. Bouguecha (2015). "Direct contact membrane
496 distillation: Capability to treat hyper-saline solution." Desalination **376**: 117-129.
497 Bouchrit, R., A. Boubakri, T. Mosbahi, A. Hafiane and S. A.-T. Bouguecha (2017). "Membrane
498 crystallization for mineral recovery from saline solution: Study case Na2SO4 crystals." Desalination
499 **412**: 1-12.
500 Chen, G., Y. Lu, X. Yang, R. Wang and A. G. Fane (2014). "Quantitative Study on
501 Crystallization-Induced Scaling in High-Concentration Direct-Contact Membrane Distillation."
502 Industrial & Engineering Chemistry Research **53**(40): 15656-15666.
503 Chen, G., Z. Wang, L. D. Nghiem, X.-M. Li, M. Xie, B. Zhao, M. Zhang, J. Song and T. He (2015).
504 "Treatment of shale gas drilling flowback fluids (SGDFs) by forward osmosis: Membrane fouling
505 and mitigation." Desalination.
506 Chen, Y., M. Tian, X. Li, Y. Wang, A. K. An, J. Fang and T. He (2017). "Anti-wetting behavior of
507 negatively charged superhydrophobic PVDF membranes in direct contact membrane distillation of
508 emulsified wastewaters." Journal of Membrane Science **535**: 230-238.
509 Chen, Y., R. Zheng, J. Wang, Y. Liu, Y. Wang, X.-M. Li and T. He (2017). "Laminated PTFE
510 membranes to enhance the performance in direct contact membrane distillation for high salinity
511 solution." Desalination **424**: 140-148.
512 Choi, C.-H., U. Ulmanella, J. Kim, C.-M. Ho and C.-J. Kim (2006). "Effective slip and friction
513 reduction in nanograted superhydrophobic microchannels." Physics of Fluids **18**(8): 087105.
514 Choi, J., Y. Choi, Y. Jang, Y. Shin and S. Lee (2017). "Effect of aeration on CaSO4 scaling in
515 membrane distillation process." Desalination and Water Treatment **90**: 7-15.
516 Choi, Y., G. Naidu, S. Jeong, S. Lee and S. Vigneswaran (2018). "Effect of chemical and physical
517 factors on the crystallization of calcium sulfate in seawater reverse osmosis brine." Desalination **426**:
518 78-87.
519 Cottin-Bizonne, C., J. L. Barrat, L. Bocquet and E. Charlaix (2003). "Low-friction flows of liquid at
520 nanopatterned interfaces." Nat Mater **2**(4): 237-240.
521 Çulfaz, P. Z., M. Haddad, M. Wessling and R. G. H. Lammertink (2011). "Fouling behavior of

522 microstructured hollow fibers in cross-flow filtrations: Critical flux determination and direct visual
523 observation of particle deposition." Journal of Membrane Science **372**(1–2): 210-218.
524 Çulfaz, P. Z., E. Rolevink, C. van Rijn, R. G. H. Lammertink and M. Wessling (2010).
525 "Microstructured hollow fibers for ultrafiltration." Journal of Membrane Science **347**(1–2): 32-41.
526 Çulfaz, P. Z., M. Wessling and R. G. H. Lammertink (2011). "Hollow fiber ultrafiltration membranes
527 with microstructured inner skin." Journal of Membrane Science **369**(1–2): 221-227.
528 Daniello, R. J., N. E. Waterhouse and J. P. Rothstein (2009). "Drag reduction in turbulent flows over
529 superhydrophobic surfaces." Physics of Fluids **21**(8): 085103.
530 Deshmukh, A., C. Boo, V. Karanikola, S. Lin, A. P. Straub, T. Tong, D. M. Warsinger and M.
531 Elimelech (2018). "Membrane Distillation at the Water-Energy Nexus: Limits, Opportunities, and
532 Challenges." Energy & Environmental Science.
533 Duong, H. C., F. I. Hai, A. Al-Jubainawi, Z. Ma, T. He and L. D. Nghiem (2017). "Liquid desiccant
534 lithium chloride regeneration by membrane distillation for air conditioning." Separation and
535 Purification Technology **177**: 121-128.
536 Edwie, F. and T.-S. Chung (2013). "Development of simultaneous membrane
537 distillation-crystallization (SMDC) technology for treatment of saturated brine." Chemical
538 Engineering Science **98**: 160-172.
539 ElSherbiny, I. M. A., A. S. G. Khalil and M. Ulbricht (2017). "Surface micro-patterning as a
540 promising platform towards novel polyamide thin-film composite membranes of superior
541 performance." Journal of Membrane Science **529**: 11-22.
542 Eykens, L., K. De Sitter, C. Dotremont, L. Pinoy and B. Van der Bruggen (2017). "Membrane
543 synthesis for membrane distillation: A review." Separation and Purification Technology **182**: 36-51.
544 Eykens, L., I. Hitsov, K. De Sitter, C. Dotremont, L. Pinoy, I. Nopens and B. Van der Bruggen (2016).
545 "Influence of membrane thickness and process conditions on direct contact membrane distillation at
546 different salinities." Journal of Membrane Science **498**: 353-364.
547 Fortunato, L., Y. Jang, J.-G. Lee, S. Jeong, S. Lee, T. Leiknes and N. Ghaffour (2018). "Fouling
548 development in direct contact membrane distillation: Non-invasive monitoring and destructive
549 analysis." Water Research **132**: 34-41.
550 Gençal, Y., E. N. Durmaz and P. Z. Çulfaz-Emecen (2015). "Preparation of patterned microfiltration
551 membranes and their performance in crossflow yeast filtration." Journal of Membrane Science **476**:

552 224-233.
553 Godoy, A. A., L. B. d. Carvalho, F. Kummrow and P. A. Z. Pamplin (2017). "Sodium chloride as a
554 reference substance for the three growth endpoints used in the Lemna minor L.(1753) test." Revista
555 Ambiente & Água **12**(1): 8-16.
556 Granick, S., Y. Zhu and H. Lee (2003). "Slippery questions about complex fluids flowing past
557 solids." Nature Materials **2**: 221-227.
558 Gryta, M. (2002). "CONCENTRATION OF NaCl SOLUTION BY MEMBRANE DISTILLATION
559 INTEGRATED WITH CRYSTALLIZATION." Separation Science and Technology **37**(15):
560 3535-3558.
561 Gryta, M. (2002). "Direct contact membrane distillation with crystallization applied to NaCl
562 solutions." CHEMICAL PAPERS-SLOVAK ACADEMY OF SCIENCES **56**(1): 14-19.
563 Gryta, M. (2008). "Fouling in direct contact membrane distillation process." Journal of Membrane
564 Science **325**(1): 383-394.
565 Gryta, M. (2010). "Desalination of thermally softened water by membrane distillation process."
566 Desalination **257**(1): 30-35.
567 Gryta, M. (2011). "The influence of magnetic water treatment on CaCO3 scale formation in
568 membrane distillation process." Separation and Purification Technology **80**(2): 293-299.
569 Gryta, M. (2016). "Degradation of Polypropylene Membranes Applied in Membrane Distillation
570 Crystallizer." Crystals **6**(4).
571 Haase, A. S., J. A. Wood, R. G. H. Lammertink and J. H. Snoeijer (2016). "Why bumpy is better: The
572 role of the dissipation distribution in slip flow over a bubble mattress." Physical Review Fluids **1**(5).
573 Hashino, M., T. Katagiri, N. Kubota, Y. Ohmukai, T. Maruyama and H. Matsuyama (2011). "Effect
574 of surface roughness of hollow fiber membranes with gear-shaped structure on membrane fouling by
575 sodium alginate." Journal of Membrane Science **366**(1–2): 389-397.
576 He, F., J. Gilron and K. K. Sirkar (2013). "High water recovery in direct contact membrane
577 distillation using a series of cascades." Desalination **323**: 48-54.
578 He, F., K. K. Sirkar and J. Gilron (2009). "Effects of antiscalants to mitigate membrane scaling by
579 direct contact membrane distillation." Journal of Membrane Science **345**(1): 53-58.
580 He, F., K. K. Sirkar and J. Gilron (2009). "Studies on scaling of membranes in desalination by direct
581 contact membrane distillation: CaCO3 and mixed CaCO3/CaSO4 systems." Chemical Engineering

582 Science **64**(8): 1844-1859.
583 He, T., M. H. V. Mulder and M. Wessling (2003). "Preparation of porous hollow fiber membranes
584 with a triple-orifice spinneret." Journal of Applied Polymer Science **87**(13): 2151-2157.
585 Hickenbottom, K. L. and T. Y. Cath (2014). "Sustainable operation of membrane distillation for
586 enhancement of mineral recovery from hypersaline solutions." Journal of Membrane Science **454**:
587 426-435.
588 Jamshidi Gohari, R., W. J. Lau, T. Matsuura and A. F. Ismail (2013). "Effect of surface pattern
589 formation on membrane fouling and its control in phase inversion process." Journal of Membrane
590 Science **446**: 326-331.
591 Jentzsch, P. V., V. Ciobotă, B. Kampe, P. Rösch and J. Popp (2011). "Origin of salt mixtures and
592 mixed salts in atmospheric particulate matter." Journal of Raman Spectroscopy **43**(4): 514-519.
593 Ji, X., E. Curcio, S. Al Obaidani, G. Di Profio, E. Fontananova and E. Drioli (2010). "Membrane
594 distillation-crystallization of seawater reverse osmosis brines." Separation and Purification
595 Technology **71**(1): 76-82.
596 Ji, Y., X.-M. Li, Y. Yin, Y.-Y. Zhang, Z.-W. Wang and T. He (2010). "Morphological control and
597 cross-flow filtration of microfiltration membranes prepared via a sacrificial-layer approach." Journal
598 of Membrane Science **353**(1-2): 159-168.
599 Jiang, X., L. Tuo, D. Lu, B. Hou, W. Chen and G. He (2017). "Progress in membrane distillation
600 crystallization: Process models, crystallization control and innovative applications." Frontiers of
601 Chemical Science and Engineering **11**(4): 647-662.
602 Julian, H., Y. Ye, H. Li and V. Chen (2018). "Scaling mitigation in submerged vacuum membrane
603 distillation and crystallization (VMDC) with periodic air-backwash." Journal of Membrane Science
604 **547**: 19-33.
605 Jung, S. Y., Y.-J. Won, J. H. Jang, J. H. Yoo, K. H. Ahn and C.-H. Lee (2015). "Particle deposition on
606 the patterned membrane surface: Simulation and experiments." Desalination **370**: 17-24.
607 Junghyun, K., K. Heejung, L. Seockheon, L. Sangho and H. Seungkwan (2017). "Membrane
608 distillation (MD) integrated with crystallization (MDC) for shale gas produced water (SGPW)
609 treatmentjournal." Desalination **403**: 172-178.
610 Kharraz, J. A., M. R. Bilad and H. A. Arafat (2015). "Flux stabilization in membrane distillation
611 desalination of seawater and brine using corrugated PVDF membranes." Journal of Membrane

612 Science **495**: 404-414.
613 Kim, J., J. Kim and S. Hong (2018). "Recovery of water and minerals from shale gas produced water
614 by membrane distillation crystallization." Water research **129**: 447-459.
615 Kim, J. U., S. Lee and T.-i. Kim (2016). "Recent Advances in Unconventional Lithography for
616 Challenging 3D Hierarchical Structures and Their Applications." Journal of Nanomaterials.
617 Kim, P., M. J. Kreder, J. Alvarenga and J. Aizenberg (2013). "Hierarchical or Not? Effect of the
618 Length Scale and Hierarchy of the Surface Roughness on Omniphobicity of Lubricant-Infused
619 Substrates." Nano Letters **13**(4): 1793-1799.
620 Kim, P., T.-S. Wong, J. Alvarenga, M. J. Kreder, W. E. Adorno-Martinez and J. Aizenberg (2012).
621 "Liquid-Infused Nanostructured Surfaces with Extreme Anti-Ice and Anti-Frost Performance." ACS
622 Nano **6**(8): 6569-6577.
623 Latorre, M. (2005). "Environmental impact of brine disposal on Posidonia seagrasses." Desalination
624 **182**(1): 517-524.
625 Lee, C., C. H. Choi and C.-J. Kim (2016). "Superhydrophobic drag reduction in laminar flows: a
626 critical review." Exp. Fluids **57-176**.
627 Lee, E.-J., A. K. An, T. He, Y. C. Woo and H. K. Shon (2016). "Electrospun nanofiber membranes
628 incorporating fluorosilane-coated TiO2 nanocomposite for direct contact membrane distillation."
629 Journal of Membrane Science **520**: 145-154.
630 Lee, J.-G., Y. Jang, L. Fortunato, S. Jeong, S. Lee, T. Leiknes and N. Ghaffour (2018). "An advanced
631 online monitoring approach to study the scaling behavior in direct contact membrane distillation."
632 Journal of Membrane Science **546**: 50-60.
633 Lee, J., C. Boo, W. H. Ryu, A. D. Taylor and M. Elimelech (2016). "Development of Omniphobic
634 Desalination Membranes Using a Charged Electrospun Nanofiber Scaffold." ACS Appl Mater
635 Interfaces **8**(17): 11154-11161.
636 Lee, Y. K., Y.-J. Won, J. H. Yoo, K. H. Ahn and C.-H. Lee (2013). "Flow analysis and fouling on the
637 patterned membrane surface." Journal of Membrane Science **427**: 320-325.
638 Li, H., H. Wang, Q. Liu, Y. Tan, N. Jiang and Y. Lin (2016). "Evaporation process for treating
639 high-salinity industrial wastewater at low temperatures and ambient pressure." Desalination and
640 Water Treatment **57**(56): 27048-27060.
641 Li, X.-M., T. He, M. Crego-Calama and D. N. Reinhoudt (2008). "Conversion of a Metastable

642 Superhydrophobic Surface to an Ultraphobic Surface." Langmuir **24**(15): 8008-8012.
643 Li, X.-M., Y. Ji, Y. Yin, Y.-Y. Zhang, Y. Wang and T. He (2010). "Origin of delamination/adhesion in
644 polyetherimide/polysulfone co-cast membranes." Journal of Membrane Science **352**(1-2): 173-179.
645 Li, X.-M., D. Reinhoudt and M. Crego-Calama (2007). "What do we need for a superhydrophobic
646 surface? A review on the recent progress in the preparation of superhydrophobic surfaces." Chemical
647 Society Reviews **36**(8): 1350-1368.
648 Li, X. M., Y. Ji, T. He and M. Wessling (2008). "A sacrificial-layer approach to prepare
649 microfiltration membranes." Journal of Membrane Science **320**(1-2): 1-7.
650 Lin, S., S. Nejati, C. Boo, Y. Hu, C. O. Osuji and M. Elimelech (2014). "Omniphobic Membrane for
651 Robust Membrane Distillation." Environmental Science & Technology Letters **1**(11): 443-447.
652 Martínez-Díez, L. and M. I. Vázquez-González (1999). "Temperature and concentration polarization
653 in membrane distillation of aqueous salt solutions." Journal of Membrane Science **156**(2): 265-273.
654 Maruf, S. H., A. R. Greenberg and Y. Ding (2016). "Influence of substrate processing and interfacial
655 polymerization conditions on the surface topography and permselective properties of
656 surface-patterned thin-film composite membranes." Journal of Membrane Science **512**: 50-60.
657 Meng, S., J. Mansouri, Y. Ye and V. Chen (2014). "Effect of templating agents on the properties and
658 membrane distillation performance of TiO2-coated PVDF membranes." Journal of Membrane
659 Science **450**: 48-59.
660 Meng, S., Y. Ye, J. Mansouri and V. Chen (2014). "Fouling and crystallisation behaviour of
661 superhydrophobic nano-composite PVDF membranes in direct contact membrane distillation."
662 Journal of Membrane Science **463**: 102-112.
663 Meng, S., Y. Ye, J. Mansouri and V. Chen (2015). "Crystallization behavior of salts during membrane
664 distillation with hydrophobic and superhydrophobic capillary membranes." Journal of Membrane
665 Science **473**: 165-176.
666 Naidu, G., S. Jeong and S. Vigneswaran (2014). "Influence of feed/permeate velocity on scaling
667 development in a direct contact membrane distillation." Separation and Purification Technology **125**:
668 291-300.
669 Naidu, G., X. Zhong and S. Vigneswaran (2018). "Comparison of membrane distillation and freeze
670 crystallizer as alternatives for reverse osmosis concentrate treatment." Desalination **427**: 10-18.
671 Nariyoshi, Y. N., C. E. Pantoja and M. M. Seckler (2016). "Evaluation of sodium chloride

crystallization in membrane distillation crystallization applied to water desalination." Brazilian Journal of Chemical Engineering **33**(3): 675-690.

Nejati, S., C. Boo, C. O. Osuji and M. Elimelech (2015). "Engineering flat sheet microporous PVDF films for membrane distillation." Journal of Membrane Science **492**: 355-363.

Nghiem, L. D., F. Hildinger, F. I. Hai and T. Cath (2011). "Treatment of saline aqueous solutions using direct contact membrane distillation." Desalination and Water Treatment **32**(1-3): 234-241.

Ramezanianpour, M. and M. Sivakumar (2014). "An analytical flux decline model for membrane distillation." Desalination **345**: 1-12.

Razmjou, A., E. Arifin, G. Dong, J. Mansouri and V. Chen (2012). "Superhydrophobic modification of TiO2 nanocomposite PVDF membranes for applications in membrane distillation." Journal of Membrane Science **415**: 850-863.

Ren, L.-F., F. Xia, V. Chen, J. Shao, R. Chen and Y. He (2017). "TiO2-FTCS modified superhydrophobic PVDF electrospun nanofibrous membrane for desalination by direct contact membrane distillation." Desalination **423**: 1-11.

Schofield, R. W., A. G. Fane and C. J. D. Fell (1987). "Heat and mass transfer in membrane distillation." Journal of Membrane Science **33**(3): 299-313.

Shannon, M. A., P. W. Bohn, M. Elimelech, J. G. Georgiadis, B. J. Mariñas and A. M. Mayes (2008). "Science and technology for water purification in the coming decades." Nature **452**: 301-310.

Shin, D. H., J. B. Park, Y. J. Kim, S. J. Kim, J. H. Kang, B. Lee, S. P. Cho, B. H. Hong and K. S. Novoselov (2015). "Growth dynamics and gas transport mechanism of nanobubbles in graphene liquid cells." Nature Communications **6**.

Shin, Y. and J. Sohn (2016). "Mechanisms for scale formation in simultaneous membrane distillation crystallization: Effect of flow rate." Journal of Industrial and Engineering Chemistry **35**: 318-324.

Tang, L., A. Iddya, X. Zhu, A. V. Dudchenko, W. Duan, C. Turchi, J. Vanneste, T. Y. Cath and D. Jassby (2017). "Enhanced Flux and Electrochemical Cleaning of Silicate Scaling on Carbon Nanotube-Coated Membrane Distillation Membranes Treating Geothermal Brines." Acs Applied Materials & Interfaces **9**(44): 38594-38605.

Tian, M., X. Li, Y. Yin, T. He and J. Liu (2015). "Preparaton of superhydrophobic membranes and their application in membrane distillation." Progress in Chemstry **27**(8): 1033-1041.

Tian, M., Y. Yin, C. Yang, B. Zhao, J. Song, J. Liu, X.-M. Li and T. He (2015). "CF4 plasma

modified highly interconnective porous polysulfone membranes for direct contact membrane distillation (DCMD)." Desalination **369**: 105-114.

Tijing, L. D., Y. C. Woo, J.-S. Choi, S. Lee, S.-H. Kim and H. K. Shon (2015). "Fouling and its control in membrane distillation-A review." Journal of Membrane Science **475**: 215-244.

Tijing, L. D., Y. C. Woo, W.-G. Shim, T. He, J.-S. Choi, S.-H. Kim and H. K. Shon (2016). "Superhydrophobic nanofiber membrane containing carbon nanotubes for high-performance direct contact membrane distillation." Journal of Membrane Science **502**: 158-170.

Truesdell, R., A. Mammoli, P. Vorobieff, F. van Swol and C. J. Brinker (2006). "Drag reduction on a patterned superhydrophobic surface." Phys Rev Lett **97**(4): 044504.

Tun, C. M., A. G. Fane, J. T. Matheickal and R. Sheikholeslami (2005). "Membrane distillation crystallization of concentrated salts—flux and crystal formation." Journal of Membrane Science **257**(1): 144-155.

Tyree, C. A., V. M. Hellion, O. A. Alexandrova and J. O. Allen (2007). "Foam droplets generated from natural and artificial seawaters." Journal of Geophysical Research: Atmospheres **112**(D12).

Tyrrell, J. W. G. and P. Attard (2001). "Images of Nanobubbles on Hydrophobic Surfaces and Their Interactions." Physical Review Letters **87**(17): 176104.

Wang, Z. X., D. Y. Hou and S. H. Lin (2016). "Composite Membrane with Underwater-Oleophobic Surface for Anti-Oil-Fouling Membrane Distillation." Environmental Science & Technology **50**(7): 3866-3874.

Wang, Z. X., J. Jin, D. Y. Hou and S. H. Lin (2016). "Tailoring surface charge and wetting property for robust oil-fouling mitigation in membrane distillation." Journal of Membrane Science **516**: 113-122.

Warsinger, D. M., A. Servi, S. Van Belleghem, J. Gonzalez, J. Swaminathan, J. Kharraz, H. W. Chung, H. A. Arafat, K. K. Gleason and J. H. V. Lienhard (2016). "Combining air recharging and membrane superhydrophobicity for fouling prevention in membrane distillation." Journal of Membrane Science **505**: 241-252.

Wei, X., B. Zhao, X.-M. Li, Z. Wang, B.-Q. He, T. He and B. Jiang (2012). "CF4 plasma surface modification of asymmetric hydrophilic polyethersulfone membranes for direct contact membrane distillation." Journal of Membrane Science **407-408**: 164-175.

Wilson, P. W., W. Lu, H. Xu, P. Kim, M. J. Kreder, J. Alvarenga and J. Aizenberg (2013). "Inhibition

of ice nucleation by slippery liquid-infused porous surfaces (SLIPS)." Physical Chemistry Chemical Physics **15**(2): 581-585.

Won, Y.-J., S.-Y. Jung, J.-H. Jang, J.-W. Lee, H.-R. Chae, D.-C. Choi, K. Hyun Ahn, C.-H. Lee and P.-K. Park (2016). "Correlation of membrane fouling with topography of patterned membranes for water treatment." Journal of Membrane Science **498**: 14-19.

Won, Y. J., J. Lee, D. C. Choi, H. R. Chae, I. Kim, C. H. Lee and I. C. Kim (2012). "Preparation and application of patterned membranes for wastewater treatment." Environ Sci Technol **46**(20): 11021-11027.

Xie, M., W. Luo and S. R. Gray (2017). "Surface pattern by nanoimprint for membrane fouling mitigation: Design, performance and mechanisms." Water Research **124**: 238-243.

Xing, L., J. Song, Z. Li, J. Liu, T. Huang, P. Dou, Y. Chen, X.-M. Li and T. He (2016). "Solvent stable nanoporous poly (ethylene-co-vinyl alcohol) barrier membranes for liquid-liquid extraction of lithium from a salt lake brine." Journal of Membrane Science **520**: 596-606.

Xue Mei Li, M. C. C. (2007). "The rough with the smooth." Chemical Science **4**: C75.

Yang, C., X.-M. Li, J. Gilron, D.-f. Kong, Y. Yin, Y. Oren, C. Linder and T. He (2014). "CF4 plasma-modified superhydrophobic PVDF membranes for direct contact membrane distillation." Journal of Membrane Science **456**: 155-161.

Yang, C., M. Tian, Y. Xie, X.-M. Li, B. Zhao, T. He and J. Liu (2015). "Effective evaporation of CF4 plasma modified PVDF membranes in direct contact membrane distillation." Journal of Membrane Science **482**: 25-32.

Yun, Y., R. Ma, W. Zhang, A. G. Fane and J. Li (2006). "Direct contact membrane distillation mechanism for high concentration NaCl solutions." Desalination **188**(1): 251-262.

Zou, T., X. Dong, G. Kang, M. Zhou, M. Li and Y. Cao (2018). "Fouling behavior and scaling mitigation strategy of CaSO4 in submerged vacuum membrane distillation." Desalination **425**: 86-93.

Highlights

1. MicroMolding phase separation (μPS) was utilized to prepare pillared hydrophobic membranes
2. Porous micropillars PVDF surface appeared superhydrophobic.
3. CF_4 plasma modification turned the surface from superhydrophobic to slippery
4. Slippery surface showed significant resistance to scaling in treating saturated NaCl solutions by membrane distillation.

11